ACCSCIENCE PUBLISHING

Journal of Seismic Exploration

ARTICLE

Porosity prediction with Bi-LSTM network for deep methane reservoirs

Qiang Guo[1], Xinyu Zhao[1], Jing Ba[2], and Cong Luo[2]*

[1]School of Resources and Geosciences, China University of Mining and Technology, Xuzhou, Jiangsu, China

[2]School of Earth Sciences and Engineering, Hohai University, Nanjing, Jiangsu, China

(This article belongs to the *Special Issue: Geophysical Inversion and Intelligent Prediction Technologies for Complex Hydrocarbon Reservoirs*)

Abstract

Quantitative prediction of petrophysical parameters, such as porosity, is crucial for the evaluation and development of coalbed methane (CBM) reservoirs. However, conventional methods based on linear assumptions and empirical formulas often fall short due to the strong heterogeneity of coal seams, complex lithologies and structures, and the highly non-linear relationship between seismic elastic parameters and reservoir properties under deep-buried conditions. While machine learning techniques have shown promise in petrophysical prediction, many existing approaches struggle to effectively capture long-range dependencies within sequential log data. This study proposes a deep learning-based method that integrates comprehensive input feature selection with a bidirectional long short-term memory (Bi-LSTM) network incorporating dropout regularization for enhanced petrophysical parameter prediction. The proposed method is designed to fully exploit the non-linear mapping between seismic elastic parameters (e.g., P-wave velocity, S-wave velocity, density, elastic impedance) and petrophysical parameter (porosity). By combining the bidirectional contextual learning capability of Bi-LSTM, the model effectively captures feature relationships within depth sequences. Comparative analysis against a fully connected neural network and a standard LSTM network demonstrates the superiority of the proposed method. The analysis also reveals the optimal feature combination and network parameter setting (sequential length, sampling interval, etc.). Results indicate that the Bi-LSTM model achieves a significant improvement in prediction accuracy, outperforming other models, and demonstrating better generalization capability in blind well tests. The method provides a reliable and effective tool for quantitative reservoir characterization, offering substantial potential for application in deep CBM exploration.

Keywords: Deep coalbed methane; Porosity prediction; Deep learning; LSTM network

***Corresponding author:**
Cong Luo
(lishang0228@163.com)

Citation: Guo Q, Zhao X, Ba J, Luo C. Porosity prediction with Bi-LSTM network for deep coalbed methane reservoirs. *J Seismic Explor*. 2025;34(6):29-44. doi: 10.36922/JSE025410087

Received: October 12, 2025

Revised: October 28, 2025

Accepted: October 30, 2025

Published online: November 19, 2025

1. Introduction

Coalbed methane (CBM), as an important component of unconventional natural gas, is currently one of the hotspots in natural gas exploration.[1] Its efficient exploration and development have become a critical pathway for increasing reserve and optimizing energy structure.[2] Petrophysical parameters of CBM reservoirs, such as porosity,

are key for characterizing reservoir quality, predicting production potential, and formulating development plans.[3,4] Previous studies calculated and predicted reservoir porosity in unknown intervals by establishing empirical formulas or simplified geological models.[5] However, due to factors such as strong coal heterogeneity, complex reservoir structure, and ambiguity in well log responses,[6,7] conventional seismic prediction methods based on linear assumptions or statistical relation are limited for detailed quantitative reservoir evaluation.[8-11] Particularly in deep CBM exploration, high temperature and pressure conditions further intensify the non-linear characteristics of rock physics relationships, making conventional prediction methods inadequate for refined reservoir characterization.[12,13] In general, the heterogeneity and complexity of CBM reservoirs cause the relationship between porosity and elastic parameters to vary significantly under different geological conditions. Traditional linear methods are unable to adapt to these variations, resulting in reduced prediction accuracy. Therefore, the accurate formulation of non-linear relation between seismic elastic parameters and petrophysical parameters is crucial for the quantitative evaluation of deep CBM reservoirs.

With the rapid development of artificial intelligence, an increasing number of machine learning methods have been applied to porosity prediction. Wu *et al.*[14] used an optimized RBF neural network to predict reservoir porosity models from well data, achieving high prediction accuracy. Ahmadi *et al.*[15] proposed a GA-LSSVM model optimized by a genetic algorithm for reservoir porosity prediction to establish more reliable static reservoir simulation models. Zerrouki *et al.*[16] employed an artificial neural network combined with a fuzzy ranking method to predict fracture porosity. Cao *et al.*[17] investigated the use of an extreme learning machine for estimating porosity and permeability in heterogeneous sandstone reservoirs. Zou *et al.*[18] utilized a random forest-based method to predict pore distribution in subsurface reservoirs.

In recent years, the rapid development of deep learning technology has demonstrated significant potential in geophysical exploration.[19-22] Deep learning techniques possess powerful feature extraction and high-dimensional data processing capabilities, enabling effective mining of deeper features from large datasets.[23-25] Their strong ability to learn complex non-linear relationships allows for more accurate approximation of the highly non-linear relationships between seismic/elastic data and target parameters.[26] Wang *et al.*[27] employed a Gaussian Mixture Model Deep Neural Network for porosity prediction, with experimental results showing its capability to reasonably estimate porosity distribution across the entire target area. Wu *et al.*[28] proposed a joint inversion method based on fluid factor and brittleness index. They developed a new P-P wave reflection coefficient approximation formula specifically for coal-measure gas reservoirs and combined it with a Bayesian inversion framework, effectively enhancing the comprehensive evaluation of gas-bearing potential and fracability.[28] Liu *et al.*[29] incorporated a low-frequency porosity model into a deep learning framework, significantly improving the trend continuity and generalization ability of porosity prediction in carbonate reservoirs. Zhang *et al.*[30] optimized the pore aspect ratio using the deep learning network aided by the Hunger Games Search algorithm to achieve joint inversion of multiple parameters in tight sandstone reservoirs, effectively improving the accuracy and reliability of rock physics modeling and inversion. Sun *et al.*[31] proposed a CNN-Transformer model aimed at improving the accuracy and generalizability of log-based porosity prediction. Tao *et al.*[32] introduced a UNet-based bidirectional neural network method to establish a mapping relationship between seismic data and porosity. While these methods have, to some extent, improved the accuracy and interpretability of porosity prediction under complex reservoir conditions, they cannot effectively handle long-range information in sequence data and fail to capture the relationships of reservoir features in deep sequences.

To address the aforementioned issues, this paper proposes a method combining input feature selection and a bidirectional long short-term memory (Bi-LSTM) network for petrophysical parameter prediction. Comparisons are made with fully connected neural (FCN) networks and unidirectional LSTM networks. The proposed method not only fully exploits the non-linear relationship between seismic elastic parameters and reservoir petrophysical parameters, but is also more sensitive to the contextual correlations within reservoir information sequences. Consequently, it can accurately capture the relationships of reservoir features within depth sequences. Furthermore, the analysis on feature selection and network parameter setting (such as sequence length and sampling interval) also provided practical guidance for deep learning-based seismic prediction of CBM reservoirs.

2. Methodologies

2.1. Fully-connected neural network

FCN network is a basic form of deep learning networks. FCN is composed of multiple layers of neurons, where each neuron in the current layer is connected to every neuron in the subsequent layer. A typical neuron receives multiple input signals, computes their weighted sum, introduces non-linearity through an activation function,

and ultimately produces an output signal. This process can be mathematically expressed as:

$$y = f(\sum_{i=1}^{n} w_i x_i + b) \quad \text{(I)}$$

Where x_i represents the input signal; w_i denotes the weight of the input signal, reflecting its importance to the neuron output; b is the bias term, which adjusts the activation threshold of the neuron; n is the dimensionality of the input features; $f(\cdot)$ is the activation function, which provides non-linear transformations; and y is the output signal of the neuron. Figure 1 shows a schematic diagram of a simple FCN network with an input feature of three dimensions, an output of one dimension, and three hidden layers.

The training of an FCN network involves four key steps.[33,34] First, in forward propagation, input feature passes through the network, undergoing weighted sums and activation functions at each layer to generate a prediction. The loss function then compares this prediction to the true value. Next, backpropagation calculates the gradient of the loss with respect to all network parameters using the chain rule. Finally, these gradients are used by an optimization algorithm to update the weights and biases. This cycle repeats until the loss converges or a maximum iteration is reached.

2.2. Long short-term memory

The long short-term memory (LSTM) network is featured by capturing long-term dependencies in sequential data by introducing a gating mechanism.[35] The core component of an LSTM is a memory cell, which contains three gates: a forget gate, an input gate, and an output gate. These gates regulate the flow of information into, within, and out of the cell, enabling the network to learn and maintain long-range dependencies. The structure of a single LSTM cell is illustrated in Figure 2.

The procedure of an LSTM network can be summarized in the following steps:

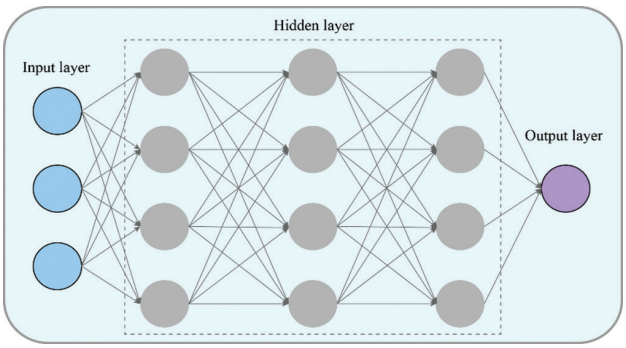

Figure 1. Structure of a simple fully connected neural network

Step 1—Compute the forget gate: This gate determines what information to discard from the cell state, indicating the degree of information retention. It is computed using a sigmoid activation function, which produces an output between 0 and 1 as:

$$f_t = \sigma(W_f \cdot [h_{t-1}, x_t] + b_f) \quad \text{(II)}$$

Where f_t is the output of the forget gate; σ is the sigmoid activation function; h_{t-1} and x_t represent the hidden state from the previous timestep and the input at the current timestep, respectively; W_f and b_f represent the weight matrix and bias term of the forget gate.

Step 2—Compute the input gate: This gate decides what new information will be stored in the cell state. The calculations take the form as:

$$i_t = \sigma(W_i \cdot [h_{t-1}, x_t] + b_i) \quad \text{(III)}$$

$$\tilde{c}_t = \tanh(W_c \cdot [h_{t-1}, x_t] + b_c) \quad \text{(IV)}$$

Where i_t is the activation vector of the input gate, determining which values to update; $\tilde{C}_t$ is the candidate value vector, determining the new values to be added; is the hyperbolic tangent activation function; W_i, W_c, b_i and b_c represent the weight matrices and bias terms for the input gate and candidate values, respectively.

Step 3—Update the cell state: The cell state, which embodies the long-term memory of the model, is updated as follows:

$$c_t = f_t \cdot c_{t-1} + i_t \cdot \tilde{c}_t \quad \text{(V)}$$

Where c_t is the current cell state; f_t is the output of the forget gate, representing the information to be discarded; c_{t-1} is the cell state from the previous timestep; i_t is the activation vector of the input gate, representing the information to be updated; and $\tilde{C}_t$ is the candidate value vector.

Step 4—Compute the output gate: This gate determines the value of the next hidden state. The hidden state contains information about the previous timestep and can be used for predicting the output at the next timestep as:

$$o_t = \sigma(W_o \cdot [h_{t-1}, x_t] + b_o) \quad \text{(VI)}$$

$$h_t = o_t \cdot \tanh(c_t) \quad \text{(VII)}$$

Where o_t is the output of the output gate; h_t is the hidden state at the current timestep; and W_o and b_o represent the weight matrix and bias term of the output gate.

In particular, the Bi-LSTM network is an extension of the standard LSTM. It incorporates two separate LSTM layers: One processing the input sequence in the forward direction

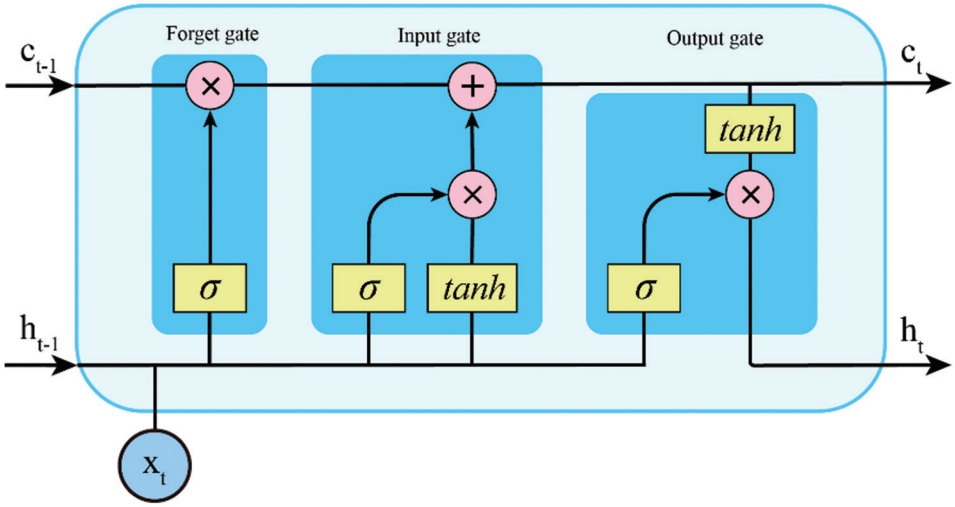

Figure 2. Structure of a single long short-term memory cell

and the other processing it in the reverse direction. The final output is generated by merging (e.g., concatenating or summing) the outputs from both directions (Figure 3). This architecture enables the model to capture dependencies from both past and future contexts simultaneously.

2.3. Activation and loss functions

The activation function is a crucial component in neural networks. Its primary role is to introduce non-linearity, enabling neural networks to learn and represent complex non-linear relationships. Common activation functions include the ReLU function, the Tanh function, and the Sigmoid function. Here, we employ the ReLU function as the activation function, which takes the form as:

$$f(x) = \max\{0, x\} \tag{VIII}$$

The loss function, aiming at training neural networks, quantifies the discrepancy between model predictions and true values, thereby driving the optimization of network parameters. Here, we employ the mean squared error to formulate the loss function, which takes the form as:

$$L_{MSE} = \frac{1}{N}\sum_{i=1}^{N}\frac{1}{d}\sum_{j=1}^{d}\left(\hat{y}_j^{(i)} - y_j^{(i)}\right)^2 \tag{IX}$$

Where L_{MSE} represents the average loss over the entire training batch, $\hat{y}_j^{(i)}$ is the predicted value, $y_j^{(i)}$ denotes the ground truth labels, N is the number of samples in the batch, and d indicates the dimensionality of the vectors.

2.4. Workflow

In this study, two different deep learning networks—FCN and LSTM—were employed for predicting petrophysical parameters from well log data. The overall workflow is illustrated in Figure 4. First, after acquiring true log data, dataset preparation was conducted, analyzing the effect of different intervals and sampling rates on prediction accuracy. Subsequently, feature selection was performed using various combinations of elastic parameters from the log data—such as S-wave velocity, P-wave velocity, density, P-to-S-wave velocity ratio, S-wave impedance, and P-wave impedance—as inputs, while using porosity as the network output, to identify the optimal combination of input features for training. Then, the prediction accuracy of the two network models was compared to determine the more suitable model for petrophysical parameter prediction, wherein the effect of sequence length of LSTM on prediction accuracy was also analyzed. Finally, blind well testing was conducted to evaluate the effectiveness of the proposed method. In addition, an attempt was made to introduce Bi-LSTM to enhance prediction accuracy and incorporate dropout to mitigate overfitting during model training.

3. Tests and applications

3.1. Dataset preparation

A total of 45,606 data points from well log measurements acquired across six wells in the study area were compiled to form the dataset. The data underwent min-max normalization, scaling all feature values to the range of 0 to 1. Outliers were removed based on the 3σ rule. These preprocessing steps ensured data quality and provided a reliable foundation for model training. The data were measured from a deep CBM reservoir in north China, with the target coal layer buried at a depth around 2000 m. It includes data from different geological settings, such as

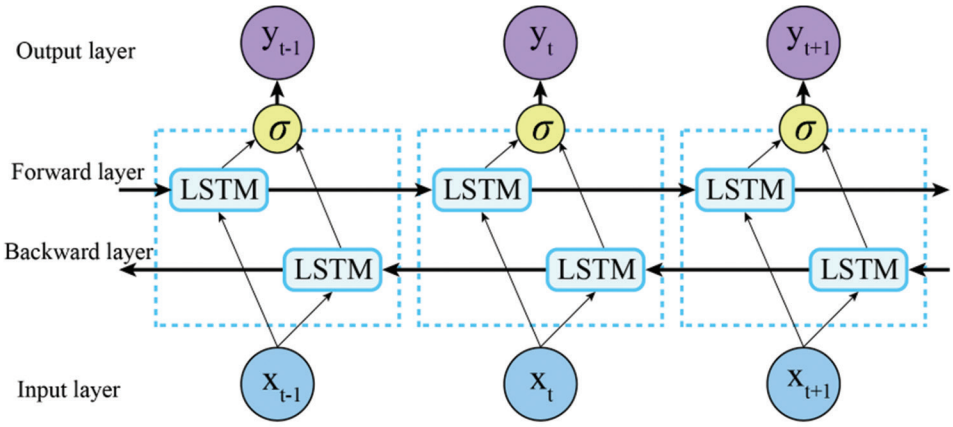

Figure 3. Structure of bidirectional long short-term memory cell

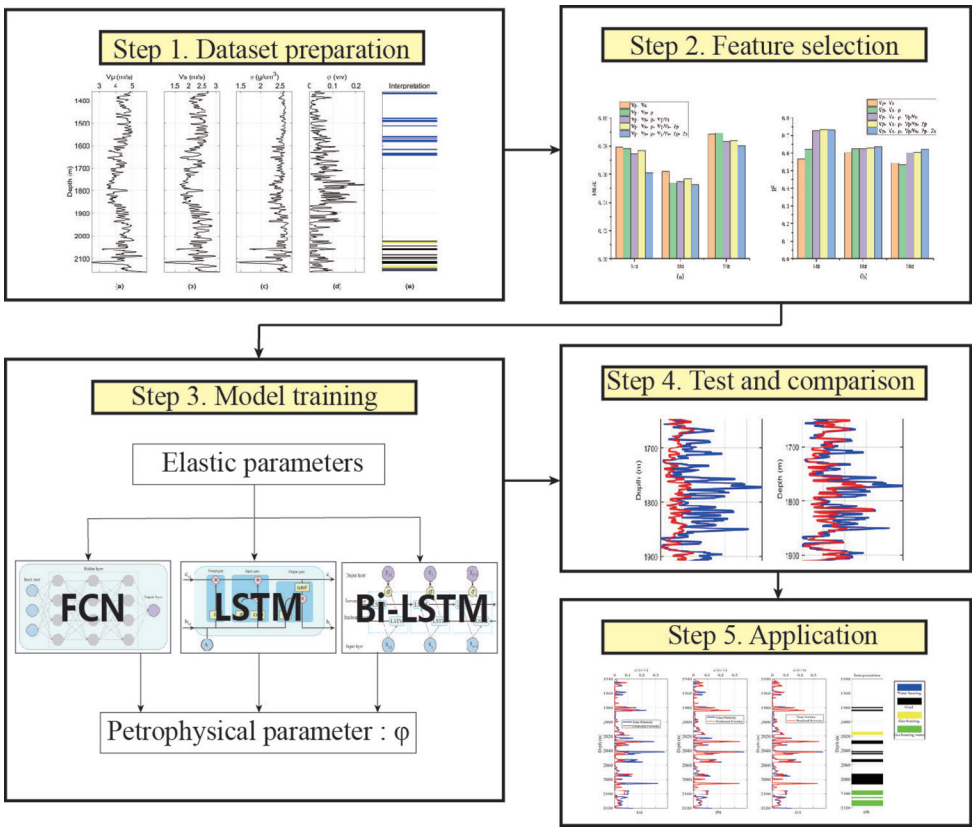

Figure 4. Workflow of the study
Abbreviations: Bi-LSTM: Bidirectional long short-term memory; FCNN: Fully connected neural network; LSTM: Long short-term memory

varying coal thickness, fracture development, and pore structures. This diversity provides a solid foundation for model training and validation, ensuring prediction accuracy and generalization under different geological conditions. The log curves and corresponding lithofacies interpretations for the selected Well B and Well C are shown in Figures 5 and 6, respectively, which exhibit a complex relationship between elastic and petrophysical properties, especially for coal sections. These data points, which include all necessary variables, are suitable for training and testing our models. This study used 80% of the data for training and 20% for validation, with random splitting to ensure consistent distribution between training and validation sets, thereby improving model generalization.

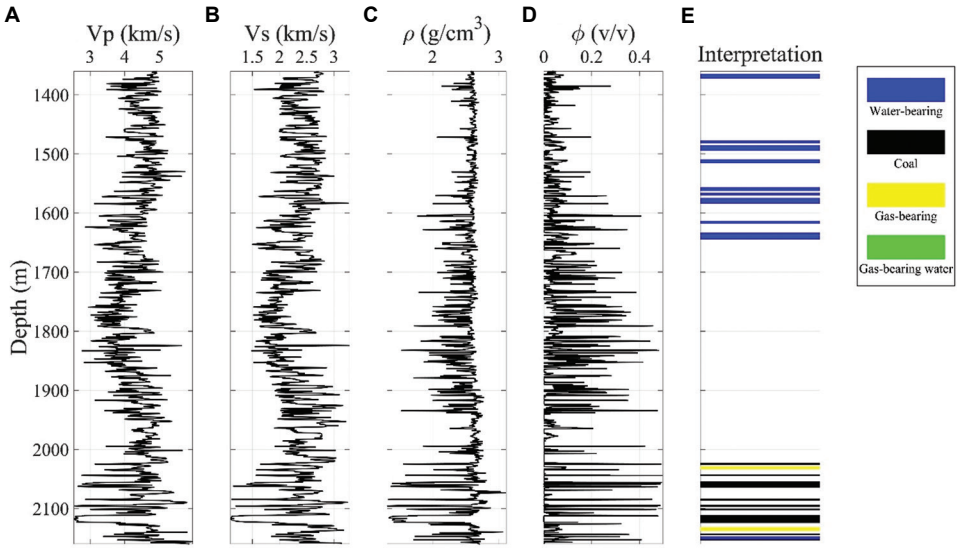

Figure 5. Log curve of P-wave velocity (A), S-wave velocity (B), density (C), porosity (D), and lithofacies interpretation result (E), for Well B

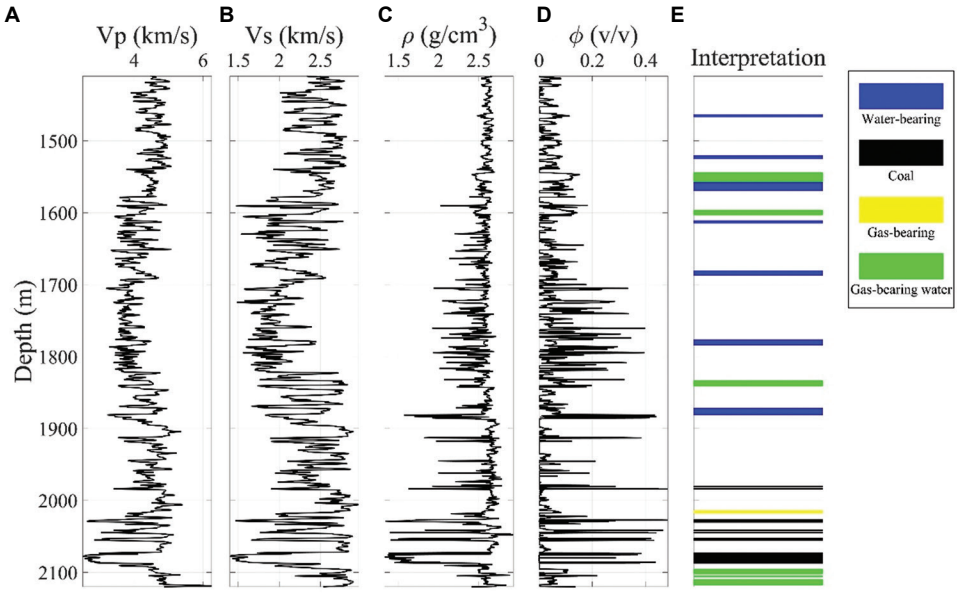

Figure 6. Log curve of P-wave velocity (A), S-wave velocity (B), density (C), porosity (D), and lithofacies interpretation result (E), for Well C

The selection of the dataset for training plays a crucial role in the accuracy and reliability of the network. We conducted a preliminary analysis on the effect of using different stratigraphic sections and sampling intervals on prediction accuracy. The analysis was performed on standard FCN networks with P-, S-wave velocities, and density as input features and porosity as output. The root mean square error (RMSE) and the coefficient of determination (R^2) from various wells were employed as evaluation metrics for prediction performance. As evidenced by the data presented in Figure 7 and Table 1, utilizing the coal section for training can effectively enhance model accuracy. It is due to the highly non-linear relation between elastic properties and porosity primarily exists in coal sections. Moreover, the analysis suggests that appropriately increasing the sampling interval can reduce the prediction error (Figure 8 and Table 2).

3.2. Feature selection

To determine the optimal input features for training, we evaluated five combinations of elastic parameters, i.e., [V_P, V_S], [V_P, V_S, ρ], [V_P, V_S, ρ, V_P/V_S], [V_P, V_S, ρ, V_P/V_S,

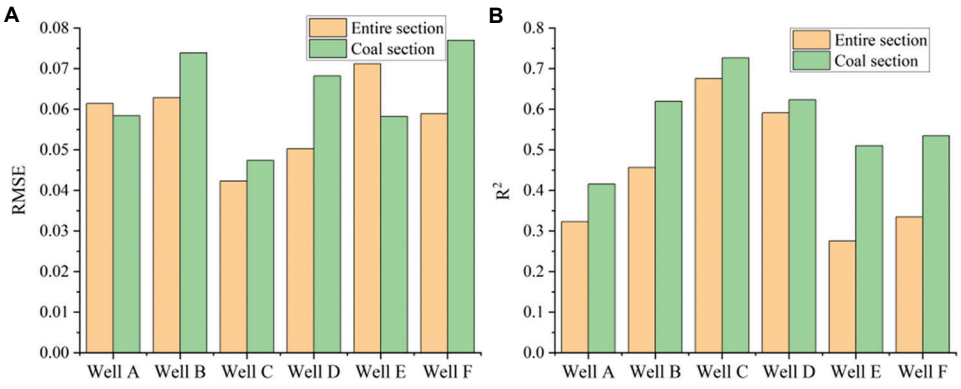

Figure 7. Prediction accuracy in term of root mean square error (A) and R^2 (B) using the training data from different stratigraphic sections

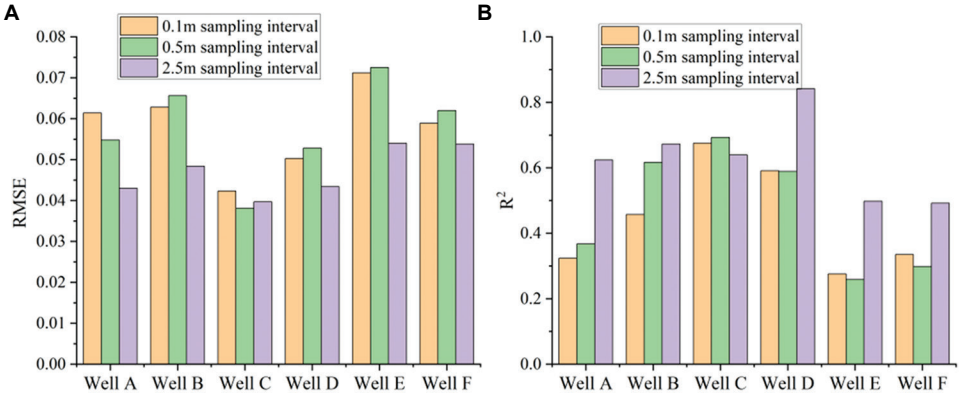

Figure 8. Prediction accuracy in term of root mean square error (A) and R^2 (B) using the training data with different sampling intervals (0.1, 0.5, and 2.5 m)

Table 1. Prediction accuracy with different stratigraphic sections

Stratigraphic section	Mean RMSE	Mean R^2
Entire section	0.0578	0.4429
Coal section	0.0639	0.5714

Abbreviation: RMSE: Root mean square error.

Table 2. Prediction accuracy with different sampling intervals

Sampling interval	Mean RMSE	Mean R^2
0.1 m	0.0578	0.4429
0.5 m	0.0576	0.4706
2.5 m	0.0470	0.6279

Abbreviation: RMSE: Root mean square error.

Z_p], and [V_P, V_S, ρ, V_P/V_S, Z_P, Z_S]. Each combination was used to train the network, and the model performance was validated using test data. When selecting certain wells for testing, the remaining wells are used to train the model. In this experiment, Wells B, D, and F within the study area were selected as the test data, respectively. The true and predicted values were recorded, and the corresponding scatter plots were shown in Figures 9-11. The RMSE and R^2 were calculated to assess the prediction accuracy and identify the optimal input feature combination. To enhance the training outcome, data sampled at an interval of 2.5 m, as suggested by the analysis in Section 3.1, was adopted as the dataset for this experiment.

As observed from the scatter plots in Figures 9-11, the prediction accuracy varies with different combinations of input features, which can be inferred by comparing the predicted against true values with the diagonal reference line. Figure 12 and Table 3 present a comparison of prediction accuracy under these different combinations. The results indicate that using Combination 5—that is, the six parameters V_P, V_S, ρ, V_P/V_S, Z_P, Z_S as input features—yields the best performance, achieving an average RMSE of 0.0647 and an average R^2 of 0.6574, which represents the highest relative accuracy among the five combinations. To better illustrate the prediction performance using different combinations, Figure 13 compares the true and predicted porosity curves for Well B when using the input feature of Combination 1 and Combination 5 with the sampling interval of 2.5 m, respectively, which indicates a significant reducing of prediction error by the optimal feature selection.

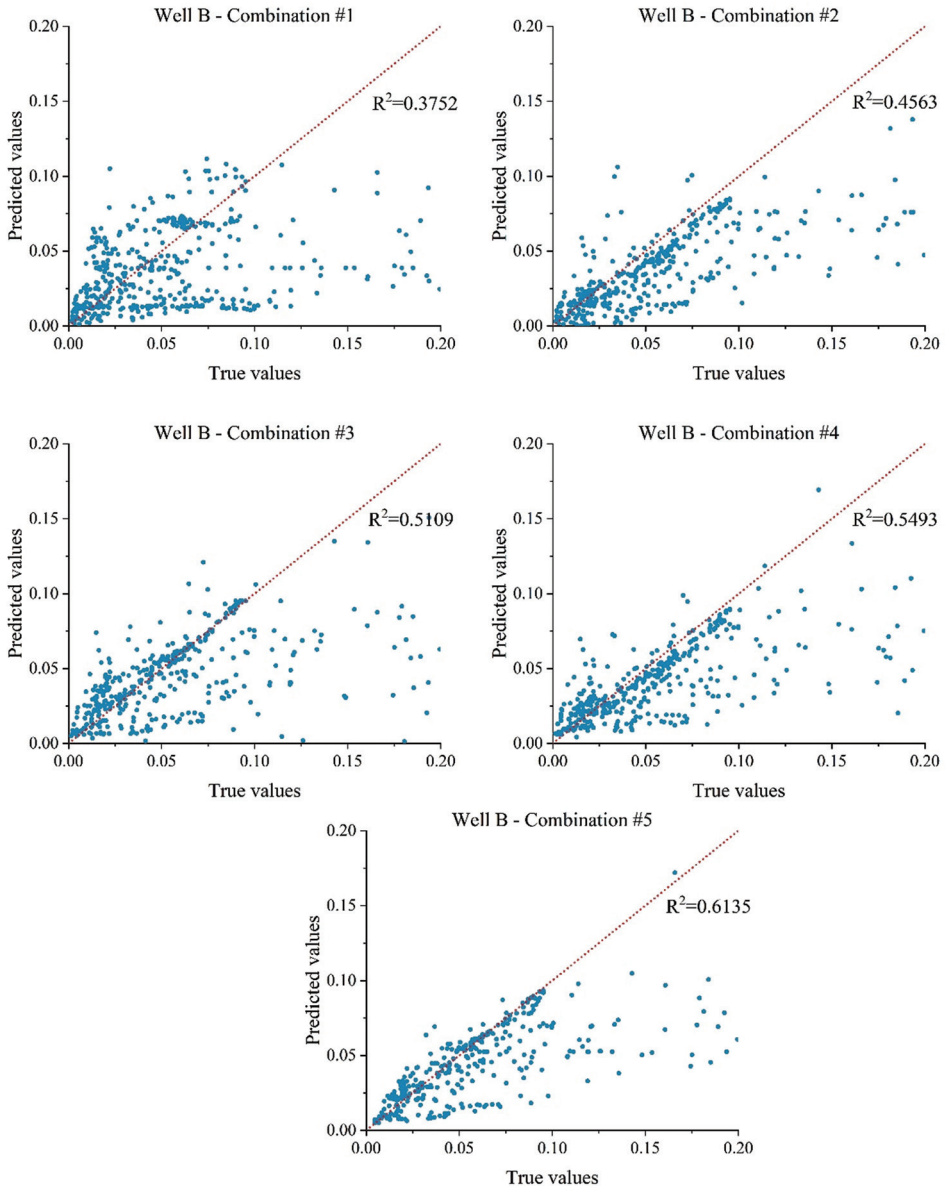

Figure 9. Prediction results with different input feature combinations for Well B

Table 3. Prediction accuracy with different combinations of input feature

Combination	Features	Mean RMSE	Mean R^2
1	[V_P, V_S]	0.0767	0.4078
2	[V_P, V_S, ρ]	0.0737	0.5117
3	[V_P, V_S, ρ, V_P/V_S]	0.0708	0.5710
4	[V_P, V_S, ρ, V_P/V_S, Z_P]	0.0724	0.6283
5	[V_P, V_S, ρ, V_P/V_S, Z_P, Z_S]	0.0647	0.6574

Abbreviation: RMSE: Root mean square error.

3.3. Model tests

To compare the performance of FCN and LSTM networks in petrophysical prediction, we conducted FCN and LSTM models and applied them to the prediction, respectively. The FCN adopts a 5-layer architecture with hidden layer sizes of 32-64-128-64-32 and uses the ReLU activation function. The LSTM model has a hidden size of 64, comprises 2 stacked layers, and is followed by a fully connected layer for output. Both networks have a dropout rate set to 0.2

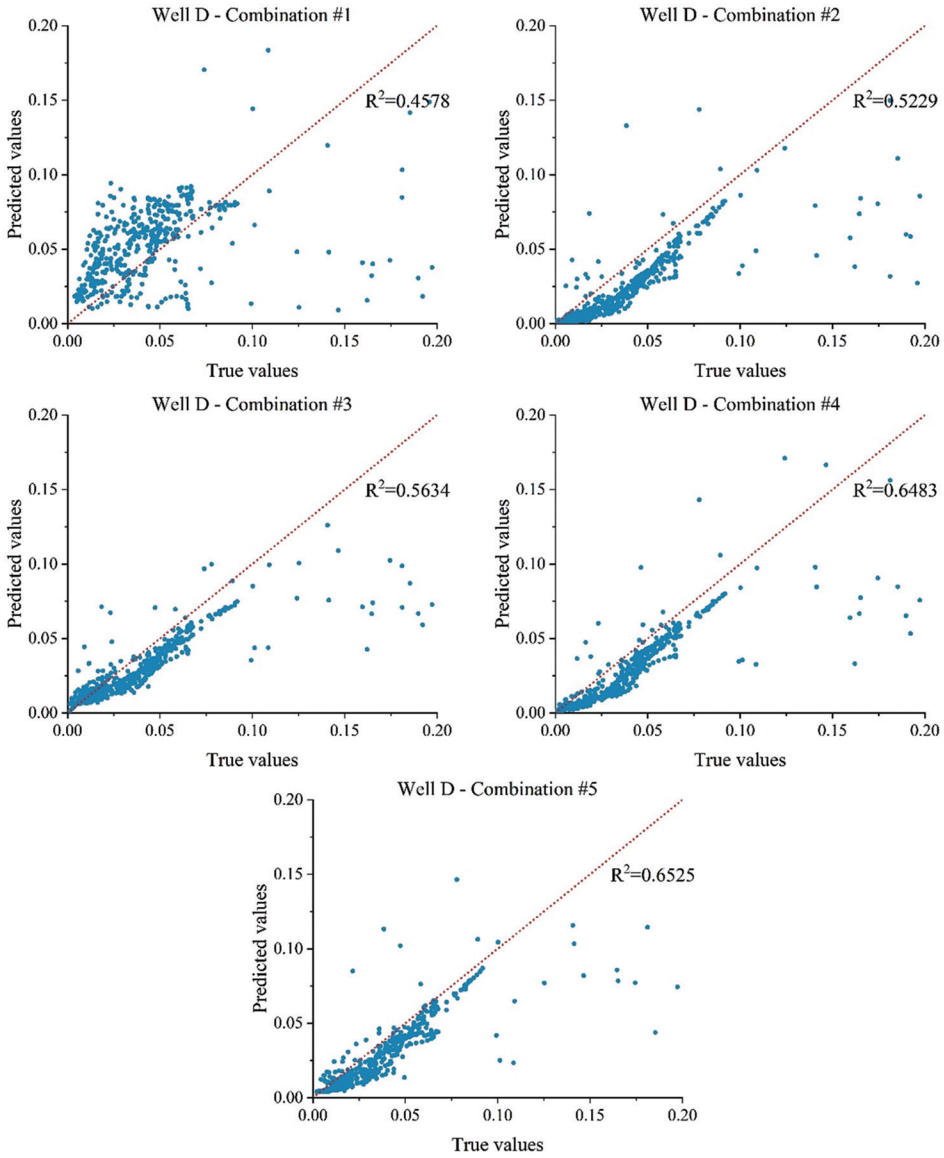

Figure 10. Prediction results with different input feature combinations for Well D

and were trained under identical conditions: Each training session employed a unified loss function, optimizer, learning rate, and batch size. We used the Adam optimizer with a learning rate of 0.001. The optimizer is crucial for efficiently and stably updating network parameters to minimize the loss. The learning rate is adjusted based on model convergence speed and stability to ensure optimal performance within a reasonable time. The models were trained by iteratively updating weights using the same training, validation, and test sets. The RMSE and R^2 for each test well were calculated to assess prediction accuracy.

As indicated by the data in Figure 14 and Table 4, the LSTM network demonstrates superior performance over the FCN network in most wells, with lower RMSE and higher R^2 values, indicating its greater suitability for petrophysical parameter prediction, especially for well-measured sequential data.

Table 4. Prediction accuracy with different network models

Network model	Mean RMSE	Mean R^2
FCN	0.0691	0.5705
LSTM	0.0621	0.6125

Abbreviations: FCN: Fully connected neural; LSTM: Long Short-Term Memory.

When training the LSTM model, the sequence length, which defines the number of sequence length in each input

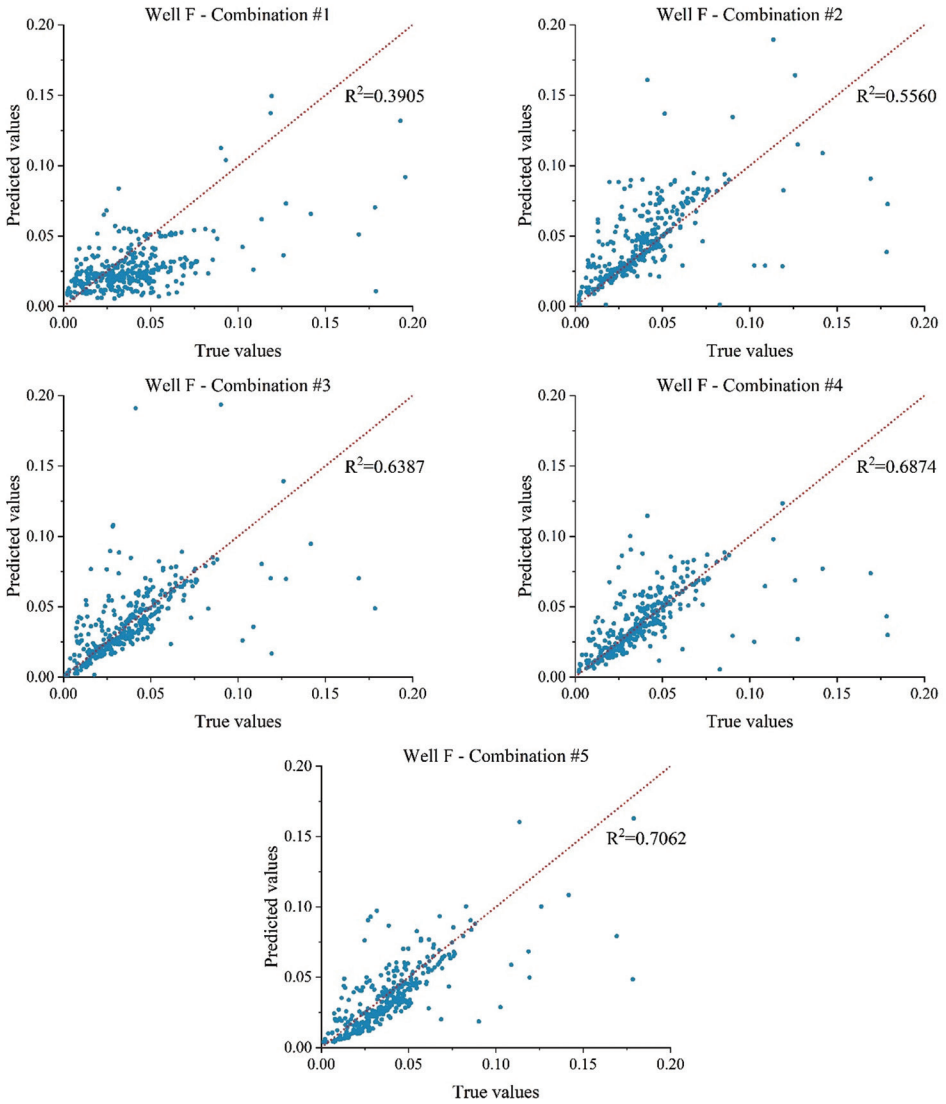

Figure 11. Prediction results with different input feature combinations for Well F

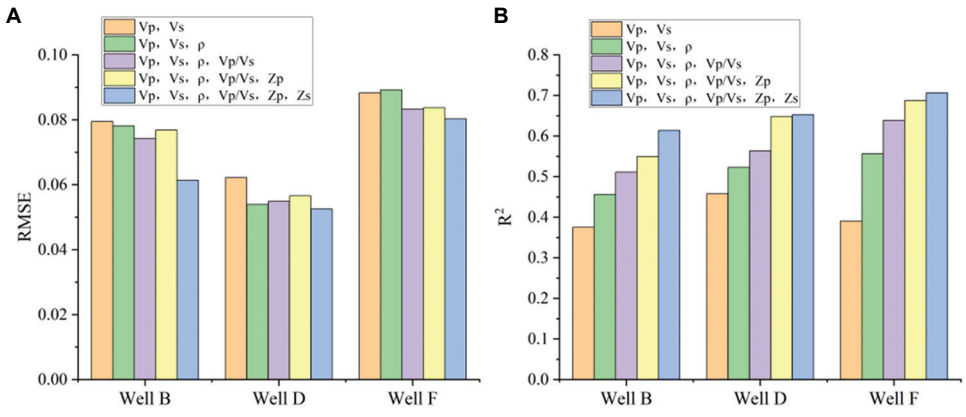

Figure 12. Prediction accuracy in term of root mean square error (A) and R^2 (B) with different combinations of input feature

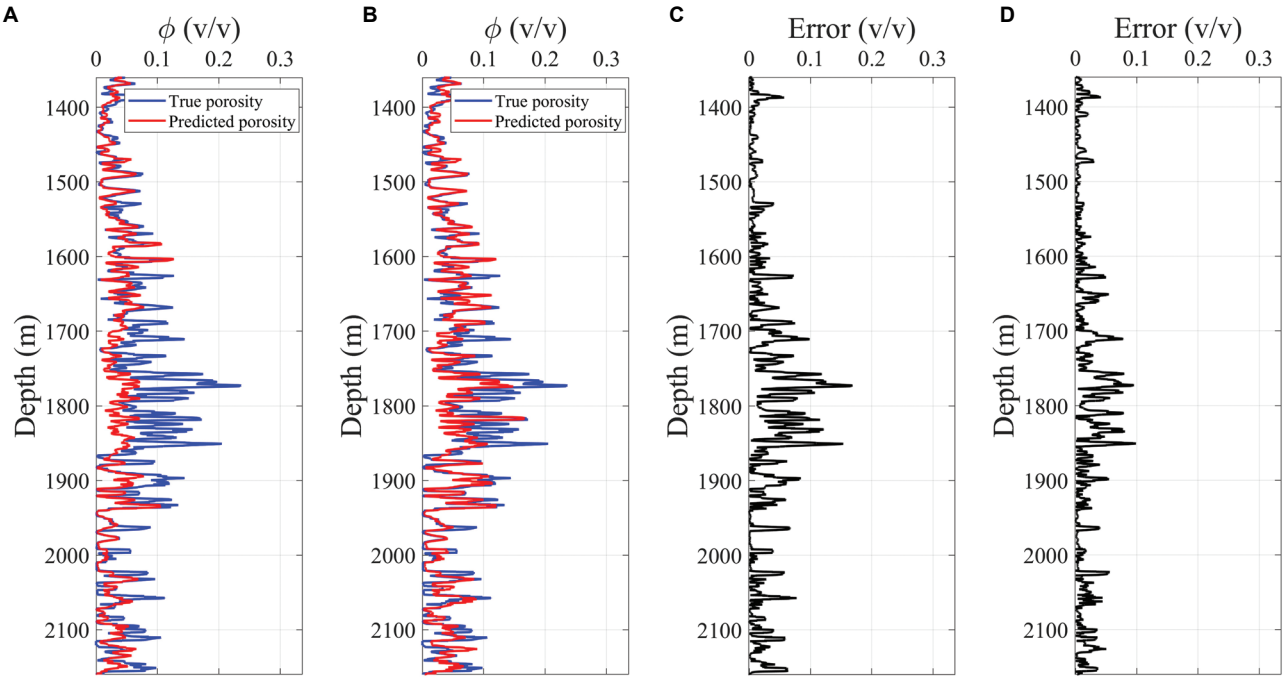

Figure 13. Comparison between the true and predicted porosity using the input feature of Combination 1 (A) and Combination 5 (B) for Well B, and their corresponding absolute residual errors (C and D)

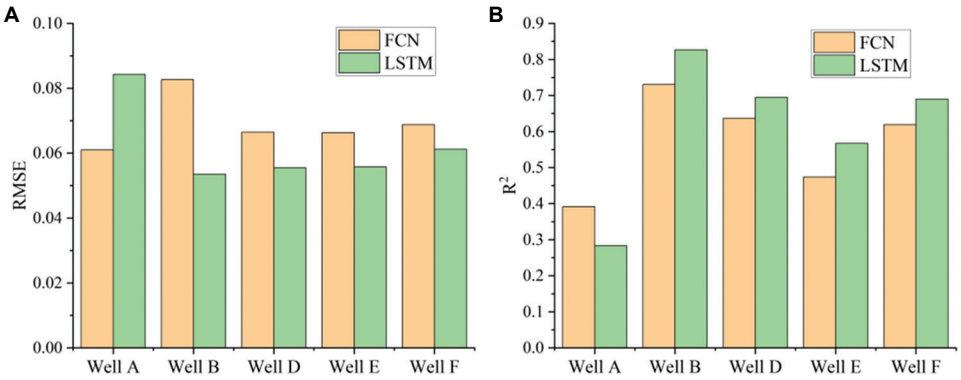

Figure 14. Prediction accuracy in term of root mean square error (A) and R^2 (B) with different network models
Abbreviations: FCN: Fully connected neural; LSTM: Long short-term memory

sequence, is a crucial parameter for data processing. Omitting this step would prevent the LSTM network from learning the influence of historical data on current values. The pore structure and fracture networks of coal seams exhibit similarity within a certain depth range (e.g., coal seams and surrounding rocks), but beyond this range, geological characteristics change significantly. The choice of sequence length is related to the geological variability with depth. A shorter sequence length may overlook the influence of geological layers, while an excessively long sequence length increases training time and may reduce generalization performance due to noise accumulation. Therefore, we analyzed the LSTM network using different sequence length values and evaluated the prediction accuracy for each test well.

As evidenced by the data in Figures 15, 16, and Table 5, a sequence length of 32 yielded the optimal performance in this test, resulting in the lowest average RMSE and the highest average R^2 across all wells. It should also be noted that the choice of sequence length significantly impacts the training duration, requiring a careful balance between sequence length and computational cost (Table 6). If the sequence length is too short, the model may fail to capture sufficient historical information, leading to issues such as underfitting and prediction lag. Conversely, an excessively long sequence

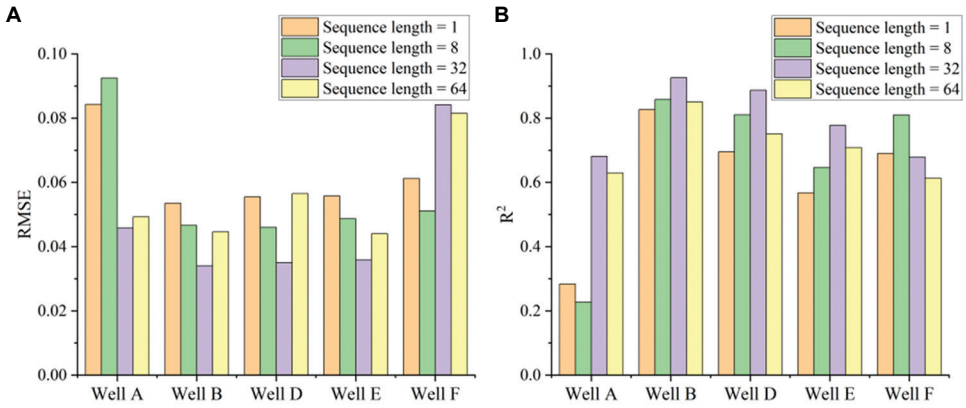

Figure 15. Prediction accuracy in term of root mean square error (A) and R^2 (B) with different sequence length for the long short-term memory network

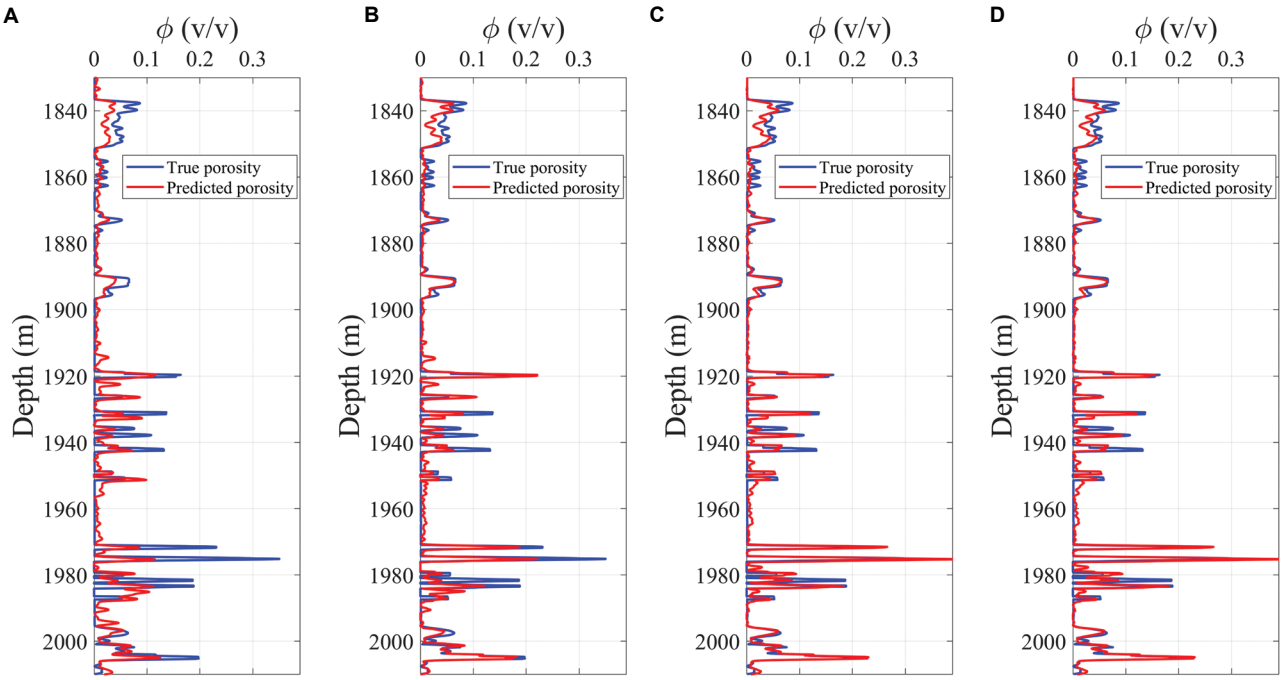

Figure 16. True and predicted porosity comparison using the long short-term memory model with sequence length of 1(A), 8 (B), 32 (C), and 64 (D), for Well D

Table 5. Prediction accuracy with different sequence length for the long short-term memory (LSTM) network

Sequence length	Mean RMSE	Mean R^2
Sequence length=1	0.0621	0.6125
Sequence length=8	0.0570	0.6704
Sequence length=32	0.0470	0.7901
Sequence length=64	0.0552	0.7105

Abbreviation: RMSE: Root mean square error.

length, while theoretically capable of incorporating richer contextual information, can cause an expansion in input dimensions and prolong the gradient backpropagation path through the LSTM hidden states. This not only substantially increases GPU memory usage and training time per iteration but may also degrade generalization performance due to accumulated noise. To reduce time costs and improve engineering feasibility, distributed training with multi-GPU acceleration can be used, or the sequence length and input dimensions can be reduced to shorten training time.

3.4. Application

To validate the effectiveness of the aforementioned method, Well C within the study area was designated as the test well,

while the remaining wells were used for training. Utilizing Combination 5 (i.e., the six parameters V_p, V_s, ρ, V_p/V_s, Z_p, and Z_s as input features), the models were trained for 100 epochs. The remaining hyperparameters were kept at their default and identical values, and the sequence length for the LSTM network was set to 32. Both the FCN and LSTM models were trained under these conditions to generate and compare their prediction results. Figures 17A and B demonstrate the superior prediction performance of the LSTM network. As indicated in Table 7, the LSTM model achieves a reduction in RMSE of approximately 43.41% and an improvement in R^2 to 0.7972 compared to the baseline.

Table 6. Comparison of training time for different sequence lengths

Model	Sequence length	Training time in seconds (100 epochs)
FCN	/	35.8
LSTM	Sequence length=1	44.2
	Sequence length=8	82.3
	Sequence length=32	246.9
	Sequence length=64	506.0

Abbreviations: FCN: Fully connected neural; LSTM: Long short-term memory.

Table 7. Prediction accuracy with different network models for Well C

Network model	Mean RMSE	Mean R^2
FCN	0.0546	0.4104
LSTM	0.0309	0.7972
Bi-LSTM	0.0279	0.8342

Abbreviations: Bi-LSTM: Bidirectional Long Short-Term Memory; FCN: Fully connected neural; LSTM: Long Short-Term Memory; RMSE: Root mean square error.

Furthermore, we employed a Bi-LSTM model to perform the prediction, while keeping all other parameters unchanged. The corresponding results are shown in Figure 17C. The Bi-LSTM model achieved an RMSE of 0.0279, representing a further reduction of 9.71% compared to the standard LSTM, and an R^2 of 0.8342, corresponding to an increase of 0.0370. In Figure 17C, it can be observed that the areas with high porosities accord with the interpreted coals at the depths around 1980 m, 2040 m, and 2080 m, which indicates the prediction could help identify coal sections in good accuracy. These results indicate that the Bi-LSTM model outperforms the standard LSTM both in terms of prediction accuracy and robustness, demonstrating its effectiveness for the task of petrophysical parameter inversion.

4. Discussion

The findings of this study indicate the potential of deep learning, especially sequence models such as LSTM and Bi-LSTM, in addressing the complex challenge of porosity prediction in deep CBM reservoirs. LSTM network inherently captures the contextual dependencies and long-

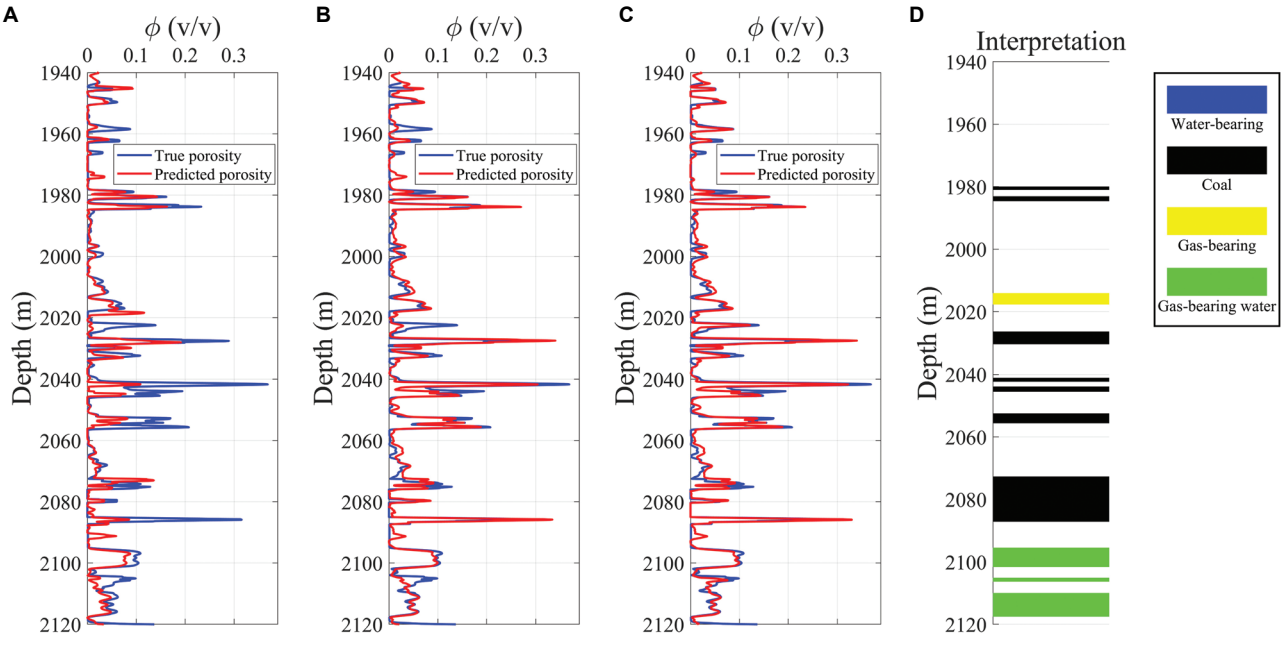

Figure 17. Prediction accuracy with FCN (A), LSTM (B), and Bi-LSTM (C), and the lithofacies interpretation (D) for Well C
Abbreviations: Bi-LSTM: Bidirectional long short-term memory; FCN: Fully connected neural; LSTM: Long short-term memory

range trends within the log curves. This capability is crucial for petrophysical prediction, as reservoir parameters at a given depth are often geologically influenced by the overlying and underlying formations. The further improvement by the Bi-LSTM model indicates that integrating information from both shallower and deeper sections leads to a more accurate prediction. Due to its bidirectional learning capability, Bi-LSTM is theoretically applicable to other sequence data-driven reservoir prediction tasks. For example, shale gas and carbonate reservoirs also have complex pore structures and non-linear relationships. With appropriate feature selection and parameter tuning, the Bi-LSTM model can be applied to porosity prediction in these reservoirs. However, it should be noted that the present study only analyzes the FCN and LSTM models, while a more comprehensive comparison with other advanced networks, such as Temporal Convolutional Networks or Transformer-based models, was not conducted. Future work should include such comparisons to more fairly evaluate the performance of Bi-LSTM model.

Overfitting remains a critical challenge in deep learning. This study employed the dropout method to mitigate overfitting by randomly dropping some neurons during training, thereby reducing the model's reliance on training data. In future research, L2 regularization will be introduced to further constrain model complexity and reduce overfitting by adding the L2 norm of weights to the loss function.

The inherent difficulties in predicting porosity in CBM reservoirs extend beyond the selection of an appropriate algorithm. The complexities of coal seams also present a fundamental task. Coal has a unique dual-porosity system, including the cleat/fracture network and the matrix pores, which governs the storage and transport mechanisms of methane. Porosity measurements and log responses are generally affected by this complex pore structure and the presence of adsorbed gas. Such inherent pore complexities are significant factors influencing the non-linear and challenging nature of the porosity prediction. However, although our data-driven model constructs the relationship between elastic parameters and porosity, it does not explicitly explain or analyze the influence of those pore complexities. A deeper investigation into how these dual-porosity characteristics manifest in the seismic elastic parameters represents a critical area for further research.

Errors may arise from model limitations and the complexity of geological characteristics. For example, the complex and variable pore structure and fracture networks in coal seams result in a highly non-linear relationship between porosity and elastic parameters. Although the Bi-LSTM model performs well in capturing such non-linear relationships, prediction errors may still occur in certain depth intervals. Future research could reduce errors by introducing more complex model structures or increasing the amount of training data.

The proposed method is primarily a data-driven approach. It takes advantage of the powerful non-linear mapping capabilities of deep learning to establish a relationship between input features and the target output, without explicitly considering the governing physical laws. It may limit the model generalizability and physical interpretability in practical applications. To address this issue, our further research will focus on developing a physics-guided deep learning model. In particular, rock physics models can provide the physical relationship between porosity and elastic parameters, offering prior knowledge for deep learning models. By incorporating a coal-specific rock physics model into the network or loss function, we aim to constrain the predictions to be not only data-consistent but also physically plausible for different CBM fields. In addition, rock physics models can supplement labeled data, compensating for the problem of overfitting of deep learning models in small sample scenarios and alleviating the impact of insufficient data.

5. Conclusion

This work proposes a deep learning-based method for predicting porosity in deep CBM reservoirs with well log data. The study investigates the input features of seismic elastic parameters for training, which leads to the optimal combination of P-wave velocity, S-wave velocity, density, and impedance for predicting porosity. The study also focuses on the analysis of network parameters such as sampling interval and sequence length, to achieve an optimal balance between prediction accuracy and computational efficiency. Tests and comparisons indicate that the LSTM network demonstrates a reduction in RMSE of approximately 43.41% and an improvement in R^2 from 0.4104 to 0.7972 compared to the FCN network. Furthermore, the proposed Bi-LSTM model not only enhances bidirectional contextual awareness but also significantly improves generalization capability. Compared to the standard LSTM, it achieved a further RMSE reduction of approximately 9.71% and increased the R^2 to 0.8342. The predictions by the Bi-LSTM model exhibit good capability in identifying potential coal layers. The proposed method provides a reliable approach for porosity prediction with well log data, which could effectively assist in seismic exploration for deep CBM reservoirs.

Acknowledgments

None.

Funding

We appreciate the support provided by the National Key Research and Development Program of China (2024YFC3015802), the National Natural Science Foundation of China (42574178 and 42374128) and the Jiangsu Provincial Science and Technology Plan Project (Natural Science Foundation of Jiangsu Province, BK20252046).

Conflict of interest

Qiang Guo and Jing Ba are Editorial Board Members of this journal but were not in any way involved in the editorial and peer-review process conducted for this paper, directly or indirectly. The authors declare they have no competing interests.

Author contributions

Conceptualization: Qiang Guo
Formal analysis: Xinyu Zhao
Investigation: Cong Luo
Methodology: Jing Ba
Writing–original draft: Qiang Guo, Xinyu Zhao
Writing–review & editing: Qiang Guo, Xinyu Zhao

Availability of data

Data are available from the corresponding author on reasonable request.

References

1. Pan J, Ge T, Liu W, *et al.* Organic matter provenance and accumulation of transitional facies coal and mudstone in Yangquan, China: Insights from petrology and geochemistry. *J Nat Gas Sci Eng*. 2021;94:104076.

   doi: 10.1016/j.jngse.2021.104076

2. Hou X, Liu S, Zhu Y, Yang Y. Evaluation of gas contents for a multi-seam deep coalbed methane reservoir and their geological controls: *In situ* direct method versus indirect method. *Fuel*. 2020;265:116917.

   doi: 10.1016/j.fuel.2019.116917

3. Gong F, Cheng J, Wang G, Peng S, Zhang Z. The effect of lamination on elastic anisotropy of primary coals under confining pressure: Experiment and theoretical modelling. *Geophys Prospect*. 2025;73(4):1228-1242.

   doi: 10.1111/1365-2478.70009

4. Gong F, Huang A, Kang W, *et al.* The influence of lamination and fracture on the velocity anisotropy of tectonic coals. *Geophysics*. 2024;89(6):MR355-MR365.

   doi: 10.1190/GEO2024-0033.1

5. Khaksar A, Griffiths CM. Porosity from sonic log in gas-bearing shale sandstones: Field data versus empirical equations. *Explor Geophys*. 1998;29(4):440-446.

   doi: 10.1071/EG998440

6. Liu X, Shao G, Yuan C, Chen X, Li J, Chen Y. Mixture of relevance vector regression experts for reservoir properties prediction. *J Petrol Sci Eng*. 2022;214:110498.

   doi: 10.1016/j.petrol.2022.110498

7. Wang P, Chen X, Wang B, Li J, Dai H. An improved method for lithology identification based on a hidden Markov model and random forests. *Geophysics*. 2020;85(6):IM27-IM36.

   doi: 10.1190/GEO2020-0108.1

8. Sang K, Yin X, Zhang F. Machine learning seismic reservoir prediction method based on virtual sample generation. *Petrol Sci*. 2021;18(6):1662-1674.

   doi: 10.1016/j.petsci.2021.09.034

9. Guo Q, Ba J, Luo C. Seismic rock-physics linearized inversion for reservoir- property and pore-type parameters with application to carbonate reservoirs. *Geoenergy Sci Eng*. 2023;224:211640.

   doi: 10.1016/j.geoen.2023.211640

10. Luo C, Ba J, Guo Q. Probabilistic seismic petrophysical inversion with statistical double-porosity Biot-Rayleigh model. *Geophysics*. 2023;88(3):M157-M171.

    doi: 10.1190/GEO2022-0288.1

11. Wang P, Cui Y, Zhou L. Multi-task learning for seismic elastic parameter inversion with the lateral constraint of angle-gather difference. *Petrol Sci*. 2024;21(6):4001-4009.

    doi: 10.1016/j.petsci.2024.06.010

12. Zhao L, Nasser M, Han D. Quantitative geophysical pore-type characterization and its geological implication in carbonate reservoirs. *Geophys Prospect*. 2013;61:827-841.

    doi: 10.1111/1365-2478.12043

13. Song L, Yin X, Zong Z, Jiang M. Semi-supervised learning seismic inversion based on Spatio-temporal sequence residual modeling neural network. *J Petrol Sci Eng*. 2022;208:109549.

    doi: 10.1016/j.petrol.2021.109549

14. Wu X, Jiang G, Wang X, *et al.* Prediction of reservoir sensitivity using RBF neural network with trainable radial basis function. *Neural Comput Appl*. 2013;22:947-953.

    doi: 10.1007/s00521-011-0787-z

15. Ahmadi MA, Ebadi M, Shokrollahi A, Majidi SMJ. Evolving artificial neural network and imperialist competitive algorithm for prediction oil flow rate of the reservoir. *Appl Soft Comput*. 2013;13(2):1082-1098.

doi: 10.1016/j.asoc.2012.10.009

16. Zerrouki AA, Aifa T, Baddari K. Prediction of natural fracture porosity from well log data by means of fuzzy ranking and an artificial neural network in Hassi Messaoud oil field, Algeria. *J Petrol Sci Eng*. 2014;115:78-89.

doi: 10.1016/j.petrol.2014.01.011

17. Cao J, Yang J, Wang Y, Wang D, Shi Y. Extreme learning machine for reservoir parameter estimation in heterogeneous sandstone reservoir. *Math Probl Eng*. 2015;2015:287816.

doi: 10.1155/2015/287816

18. Zou C, Zhao L, Xu M, Chen Y, Geng J. Porosity prediction with uncertainty quantification from multiple seismic attributes using Random Forest. *J Geophys Res Solid Earth*. 2021;126:e2021JB021826.

doi: 10.1029/2021JB021826

19. Elkatatny S, Mahmoud M, Tariq Z. New insights into the prediction of heterogeneous carbonate reservoir permeability from well logs using artificial intelligence network. *Neural Comput Appl*. 2018;30(9):2673-2683.

doi: 10.1007/s00521-017-2850-x

20. Wu X, Shi Y, Fomel S. FaultNet3D: Predicting fault probabilities, strikes, and dips with a single convolutional neural network. *IEEE Trans Geosci Remote Sens*. 2019;57(11):9138-9155.

doi: 10.1109/TGRS.2019.2925003

21. Wang P, Xu H, Peng Z, Wang Z, Yang M. Application of data augmentation based on generative adversarial network in impedance inversion. *J Seismic Explor*. 2023;32(2):155-168.

22. Behnia AMO, Reza M, Ali M. A new approach for seismic inversion with GAN algorithm. *J Seismic Explor*. 2024;33(3):1-36.

23. Suraj P, Omer S, Aditya N, *et al.* Model fusion with physics-guided machine learning: Projection-based reduced-order modeling. *Phys Fluids*. 2021;33(6):067123.

doi: 10.1063/5.0053349

24. Xu M, Zhao L, Gao S, Zhu X, Geng J. Joint use of multiseismic information for lithofacies prediction via supervised convolutional neural networks. *Geophysics*. 2022;87(5): 151-162.

doi: 10.1190/GEO2021-0554.1

25. Gao S, Xu M, Zhao L, Chen Y, Geng J. Seismic predictions of fluids via supervised deep learning: Incorporating various class-rebalance strategies. *Geophysics*. 2023;88(4):185-200.

doi: 10.1190/GEO2022-0363.1

26. Yu S, Ma J. Deep learning for geophysics: Current and future trends. *Rev Geophys*. 2021;59:e2021RG000742.

doi: 10.1029/2021RG000742

27. Wang Y, Niu L, Zhao L, *et al.* Gaussian mixture model deep neural network and its application in porosity prediction of deep carbonate reservoir. *Geophysics*. 2022;87(2):59-72.

doi: 10.1190/GEO2020-0740.1

28. Wu H, Wu R, Zhang P, Huang Y, Huang Y, Dong S. Combined fluid factor and brittleness index inversion for coal-measure gas reservoirs. *Geophys Prospect*. 2022;70:751-764.

doi: 10.1111/1365-2478.13172

29. Liu J, Zhao L, Xu M, Zhao X, You Y, Geng J. Porosity prediction from prestack seismic data via deep learning: Incorporating a low-frequency porosity model. *J Geophys Eng*. 2023;20(5):1016-1029.

doi: 10.1093/jge/gxad063

30. Zhang J, Liu Z, Zhou Y, Ai H, Han H. Joint inversion method of rock physics based on hunger games search correction and Bi-LSTM. *IEEE Trans Geosci Remote Sens*. 2024;62:5914310.

31. Sun Y, Pang S, Zhang J, Zhang Y. Porosity prediction through well logging data: A combined approach of convolutional neural network and transformer model (CNN-transformer). *Phys Fluids*. 2024;36(2):026604.

doi: 10.1063/5.0190078

32. Tao B, Zhou H, Chen L, Liu B, Wang R, Liu X. Porosity prediction based on stochastic modeling and facies-controlled dataset constrained by seismic attribute. *IEEE Geosci Remote Sens Lett*. 2025;22:1-5.

doi: 10.1109/LGRS.2025.3580778

33. Ashraf M, Robles WRQ, Kim M, Ko YS, Yi MY. A loss-based patch label denoising method for improving whole-slide image analysis using a convolutional neural network. *Sci Rep.* 2022;12:1392.

doi: 10.1038/s41598-022-05001-8

34. Gao Z, Li C, Yang T, Pan Z, Gao J, Xu Z. OMMDE-Net: A deep learning-based global optimization method for seismic inversion. *IEEE Geosci Remote Sens Lett*. 2021;18:208-212.

doi: 10.1109/LGRS.2020.2973266

35. Hochreiter S, Schmidhuber J. Long short-term memory. *Neural Comput*. 1997;9:1735-1780.

doi: 10.1162/neco.1997.9.8.1735